Biophysical Journal Volume 100

Supporting Material

Title: Feed-forward and Feed-backward Amplification Model from Cochlear

Authors: Yong-Jin Yoon, Charles R. Steele, and Sunil Puria

Feed-forward and Feed-backward Amplification Model from Cochlear Cytoarchitecture: An Interspecies Comparison

Yong-Jin Yoon[†], Charles R. Steele[†], and Sunil Puria[†, ‡],

[†]*Department of Mechanical Engineering, Stanford University, Durand Building, California 94305-4035, USA*
[‡]*Department of Otolaryngology-Head and Neck Surgery, Stanford University, Stanford, California 94305, USA*

SUPPORTING MATERIAL

This supporting material section describes the methods, parameters, and some results corresponding to the passive cochlear model upon which the active push-pull mechanics of the outer hair cell amplification is built and described in the main text. In addition, the pressure gain for the passive and active cases is reported.

METHODS

Theoretical Background

Overall features and dimensions of the 3-D hydrodynamic model used in this study are described in Figure S1. This is a standard "box" model of the cochlea. Deviations from the actual cochlea include the straight walls, drastic simplification of the basal hook region, absence of Reissner's membrane and the organ of Corti, symmetric scalae, and only one significant transverse mode of BM deformation. Nevertheless results from an asymptotic WKB solution method for the differential equations describing the mechanics of the cochlea, with physical values for the BM and the 3-D viscous fluid, show the passive behavior well (1). The current model incorporates the scala areas found in 3-D reconstructions of μCT scans. In (2,3) a direct integration of the 3-D equations provides a reduction to a single second-order wave equation, with the speed dependent on the 3-D details. This is convenient for either numerical or asymptotic analysis. However, in (4) better results are found by returning to the method in (1) of equating the time-averaged kinetic and potential energies of the conservative system. The extension to a viscous-elastic system is validated in (4). The mathematical formulation for just the passive model is described next.

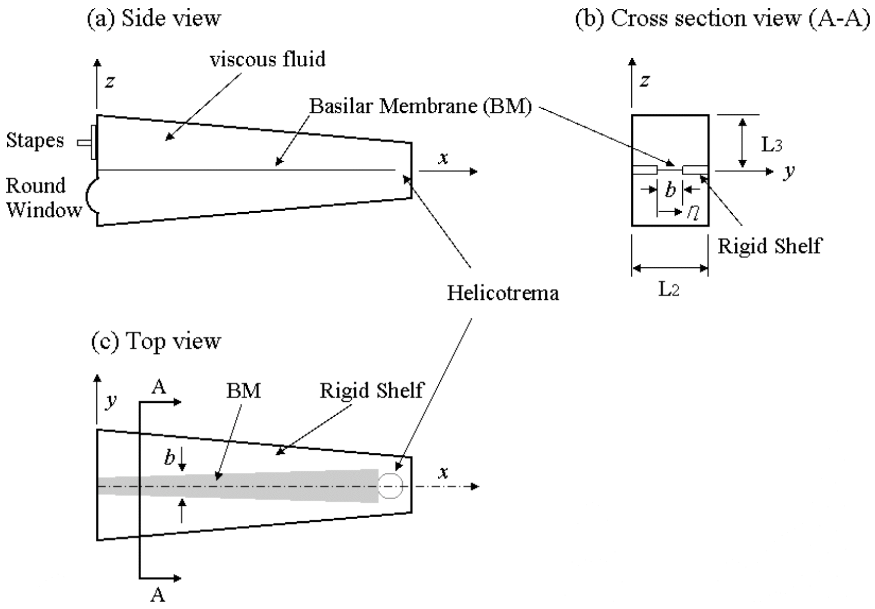

Figure S1: Schematic drawing of the geometric layout of the biophysical cochlear model. Distances are parameterized in Cartesian coordinates {x, y, z} representing the distance from the stapes, the distance across the scala width, and the height above the basilar membrane, respectively. (a) Side view; (b) Cross-sectional view (A-A); and (c) top view of the cochlear model.

Methods

Time-averaged Lagrangian for the passive model

Time-averaged kinetic energy of the cochlear fluid (T_f)

The fluid velocity vector $\underline{V} = \dot{u}\hat{i} + \dot{v}\hat{j} + \dot{w}\hat{k}$ in the scala vestibuli and scala tympani can be decomposed into the gradient of the scalar potential ϕ and the curl of rotational potential $\underline{\psi}$ as

$$\underline{V} = \nabla\phi + \nabla\times\underline{\psi}\,, \tag{A1}$$

where the fluid velocities in the *x, y,* and *z* directions, respectively, are $\dot{u}$, $\dot{v}$, and $\dot{w}$. The displacement components are *u, v,* and *w,* and dots above the letters denote differentiation with respect to time. To simplify the development process, we assume the displacement profile of the BM in harmonic motion, w_p, to be

$$w_p(x,\eta,t) = e^{i\theta}W(x)\eta(\xi)\,, \tag{A2}$$

where the phase $\theta = \omega t - \int_0^x n(x)dx$ (in which ω is the frequency and n is the wave number) and $\eta(\xi) = \sin\left(\frac{\pi\xi}{b}\right)$ for simply-supported edges (b is the width of BM). The coordinate ξ is the y co-

ordinate which has its origin at one edge of the BM. $W(x)$ is the amplitude of the envelope.

The continuity condition for an incompressible viscous fluid flow is given by the Laplace's equation on the scalar potential ϕ (with $\Delta\phi = 0$), which satisfies the rigid wall boundary conditions at $y = 0$, $y = L_2$, and $z = L_3$, where the normal fluid displacements are zero. Thus, for the fluid, the appropriate boundary conditions for the upper duct are

$$v = 0 \text{ at } y = 0 \text{ and } y = L_2,$$

$$w = 0 \text{ at } z = L_3, \text{ and} \tag{A3}$$

$$w = \begin{pmatrix} w_p & (0 \le \xi \le b) \\ 0 & (otherwise) \end{pmatrix} \text{ at } z = 0.$$

A functional form of ϕ that satisfies the above boundary conditions is

$$\phi(x,y,z,t) = e^{i\theta} \sum_{j=0}^{\infty} R_j(x) \cos\left(\frac{j\pi y}{L_2}\right) \cosh\left(\tau_j(x)(z - L_3)\right), \tag{A4}$$

where $\tau_j(x) = \sqrt{n^2 + \left(\frac{j\pi}{L_2}\right)^2}$.

The linearized Navier-Stokes equations for no body force can be combined with Eq. A1 to yield

$$\rho_f \frac{\partial \underline{\psi}}{\partial t} = \mu \nabla^2 \underline{\psi}, \tag{A5}$$

in which μ is the dynamic viscosity of the fluid and ρ_f is the mass density of the fluid.
Due to the low viscosity of the fluid, the boundary layers are localized such that the boundary layers at the rigid walls have no significant effects on the partition motion. Hence, only the boundary layer at the partition is considered. For exponential decay with distance above the partition, the solution to Eq. A5 which is significant near the partition (z=0), is

$$\underline{\psi}(x,y,z,t) = \sum_{j=0}^{\infty} R_j(x) \cosh\left(\kappa_j(x) L_3\right) \left[\left(\frac{-j\pi}{\beta_j L_2}\right) \sin\left(\frac{j\pi y}{L_2}\right) \hat{i} + \left(\frac{i\lambda}{\beta_j}\right) \cos\left(\frac{j\pi y}{L_2}\right) \hat{j} \right] e^{(-\beta_j z + i\theta)}, \tag{A6}$$

where $\kappa_j(x) = \sqrt{\tau_j^2 - i\omega \frac{\rho_f}{\mu}}$.

Note that vector field $\underline{\psi}$ describes the rotational component of the fluid displacement field due to viscosity. A steady-state harmonic excitation with frequency ω is applied at the stapes.

With Eq. A6, the three velocity components given by Eq. A1 become

$$\dot{u}(x,y,z,t) = -ine^{i\theta}\sum_{j=0}^{\infty} R_j(x)\left[\cosh\left(\tau_j(z-L_3)\right)-\cosh\left(\tau_j L_3 e^{-\beta_j z}\right)\right]\cos\left(\frac{j\pi y}{L_2}\right), \tag{A7a}$$

$$\dot{v}(x,y,z,t) = -e^{i\theta}\sum_{j=0}^{\infty} R_j(x)\left(\frac{j\pi}{L_2}\right)\left[\cosh\left(\tau_j(z-L_3)\right)-\cosh\left(\tau_j L_3 e^{-\beta_j z}\right)\right]\sin\left(\frac{j\pi y}{L_2}\right), \text{ and} \tag{A7b}$$

$$\dot{w}(x,y,z,t) = e^{i\theta}\sum_{j=0}^{\infty} R_j(x)\tau_j(x)\left[\sinh\left(\tau_j(z-L_3)\right)+\beta_j^{-1}\tau_j\cosh\left(\tau_j L_3 e^{-\beta_j z}\right)\right]\cos\left(\frac{j\pi y}{L_2}\right). \tag{A7c}$$

Applying the third boundary condition in Eq. 3 to the normal displacement calculated from Eq. A7c yields $R_j(x)$, which allows the fluid to match the arbitrary displacement on the BM. Following the Fourier series inversion yields

$$R_j(x) = \frac{-i\omega W(x)A_j}{\tau_j L_2\sinh(\tau_j L_3)\left(1-\beta_j^{-1}\tau_j\coth(\tau_j L_3)\right)}\times\begin{Bmatrix}1 & (j=0)\\ 2 & (j=1,2,...)\end{Bmatrix}, \tag{A8}$$

where $A_j = \int_0^b \eta(\xi)\cos\left(j\pi y/L_2\right)d\xi$.

With the coefficients $R_j(x)$ known, the pressure distribution in the cochlear fluid, p, can be obtained from the linearized Navier-Stokes equations as

$$p = -\rho_f\frac{\partial\phi}{\partial t} = -i\rho\omega\phi. \tag{A9}$$

Combining Eq. A4, Eq. A6, and Eq. A9 yields the 3-D intracochlear pressure distributions for the traveling wave

$$p(x,y,z,t) = -i\rho_f\omega e^{i\theta}\sum_{j=0}^{\infty} R_j(x)\cos\left(\frac{j\pi y}{L_2}\right)\cosh\left(\tau_j(x)(z-L_3)\right). \tag{A10}$$

For the pressure acting on the BM, only the first transverse mode of deflection, Eq. A2, and the corresponding first mode of the pressure are considered. By setting z=0 in Eq. A10, the normal stress on the BM can be written as

$$p(x,y,0,t) = -i\rho_f\omega e^{i\theta}\sum_{j=0}^{\infty} R_j(x)\cos\left(\frac{j\pi y}{L_2}\right)\cosh\left(\tau_j(x)L_3\right) = e^{i\theta}P\eta(\xi), \tag{A11}$$

where

$$P = \frac{-i\rho_f \omega \sum_{j=0}^{\infty} R_j(x) A_j(x) \cosh(\tau_j(x) L_3)}{\int_0^b \eta^2(\xi) d\xi} = -\rho_f \omega^2 W(x) H_{eq}, \quad \text{(A12)}$$

and where H_{eq} is the equivalent fluid thickness.

The kinetic energy of the fluid in both ducts averaged over one cycle in time is

$$T_f = \int_0^b \frac{1}{2\pi} \int_0^{2\pi} \rho_f H_{eq} \dot{w}_p^2 d\theta d\xi, \quad \text{(A13)}$$

which by symmetry is twice that of the upper duct. With the use of Eq. A2, Eq. A13 yields

$$T_f = \frac{1}{2} \rho_f \omega^2 H_{eq} W^2(x) \int_0^b \eta^2(\xi) d\xi. \quad \text{(A14)}$$

Time-averaged kinetic energy of the BM plate (T_p)

For the BM plate, the time-averaged kinetic energy density (T_p) is

$$T_p = \frac{1}{2\pi} \int_0^{2\pi} \int_0^b \frac{1}{2} \rho_p h \dot{w}_p^{\,2} d\xi d\theta, \quad \text{(A15)}$$

which, when combined with Eq. A2, becomes

$$T_p = \frac{1}{4} \rho_p \omega^2 h W(x)^2 \int_0^b \eta^2(\xi) d\xi, \quad \text{(A16)}$$

where ρ_p and h are the mass density and thickness of the BM plate, respectively.

Time-averaged potential energy of the BM plate (V_p)

For the BM plate, the time-averaged potential energy (V_p) is

$$V_p = \int_0^b \frac{1}{2\pi} \int_0^{2\pi} \frac{D}{2} \left\{ \left[\left(\frac{\partial^2 w_p}{\partial x^2} \right)^2 + 2\nu \left(\frac{\partial^2 w_p}{\partial x^2} \right) \left(\frac{\partial^2 w_p}{\partial \xi^2} \right) + 2(1-\nu) \left(\frac{\partial^2 w_p}{\partial x \partial \xi} \right)^2 \right] + \left(\frac{\partial^2 w_p}{\partial \xi^2} \right)^2 \right\} d\theta d\xi, \quad \text{(A17)}$$

in which $D = E_{22} \frac{f h^3}{(1-\nu^2)}$, where E_{22} is the Young's modulus in the transverse direction, h is the effective BM thickness, ν is Poisson's ratio, and f is the fiber volume fraction of the BM, which decreases from 3% to 0.7% along the longitudinal direction of the cochlea from the base to the apex (5).

The BM plate has orthotropic properties since the BM contains transverse fibers in the radial direction (6). With consideration for the orthotropic BM, integration of Eq. A17 yields

$$V_p = K\Gamma W(x)^2 \left(\int_0^b \eta^2(\xi) d\xi \right), \quad \text{(A18)}$$

where for simply supported edges

$$\Gamma = \frac{2b}{\pi^2}\left\{1 + k_x\left[2\left(\frac{nb}{\pi}\right)^2 + \left(\frac{nb}{\pi}\right)^4\right]\right\}, \tag{A19}$$

in which k_x is the ratio of the effective elastic modulus in the longitudinal direction (E_{11}) to the modulus in the transverse direction (E_{22}).

The stiffness K, which is the static stiffness of the plate under uniform pressure, is

$$K = \left(\frac{\pi^6}{8}\right)\left(\frac{D}{b^5}\right). \tag{A20}$$

Phase relation

By equating the time-averaged kinetic and potential energies of the system, the time-averaged Lagrangian density is obtained:

$$L = T_f + T_p - V_p = F(n,\omega)W^2(x)\left(\int_0^b \eta^2(\xi)d\xi\right) = 0, \tag{A21}$$

which gives the phase relation for the active case, $F(n,\omega)=0$. The amplitude function $W(x)$ is computed from

$$W(x) = C\left(\frac{\partial F(n,\omega)}{\partial n}b\right)^{-1/2}. \tag{A22}$$

The total amplitude of Eq. A22 is, of course, highly dependent on the imaginary part of the wave number n.

Table S1: Material properties for the cochlear model

Region	Symbol	Description		Value
Basilar Membrane	ρ_p	Density of the BM plate		1.0 x 10^3 kg/m^3
	E_{11}	Young's modulus	longitudinal direction	1.0 x 10^{-4} GPa
	E_{22}		radial direction	1.0 GPa
	E_{12}		coupling term	E_{12} = 0.0 GPa
	ν	Poisson's ratio		ν = 0.5
Scala Fluid	ρ_f	Density of the fluid		1.0 x 10^3 kg/m^3
	μ	Fluid viscosity		0.7 x 10^{-3} Pa s

The input parameters were the nominal material properties in Table S1 (7); the scala vestibuli area, BM width, and BM thickness as functions of distance from the stapes (Figure 2); and the length of the cochlea, stapes footplate area (A_{st}), length of OHCs (8), and fiber volume fraction (2) in Table S2, based on anatomical measurements for gerbil (9-12), chinchilla (13, 14), cat (15-17), and human (18-21).

Table S2: Dimensions of the interspecies cochlear models

	Gerbil	Chinchilla	Cat	Human
Length of the cochlea (*mm*)	12 (9)	18 (14)	25 (16)	35 (18)
Stapes footplate area (mm^2)	0.62 (10)	0.7 (13)	1.26 (17)	3.21 (21)
Length of outer hair cell (μm)	25-65 (from stapes to apex, (8))			
Fiber volume fraction (%)	3-0.7 (from stapes to apex, (2))			

Forty terms were used in the Fourier expansion across the width of the scala. The calculation of the Fourier expansion with eighty terms showed no difference. Running on a laptop Intel Pentium Ⅸ (3.40 GHz) processor, the average time taken for a single harmonic excitation simulation was around one second. This method provides a fast and efficient solution compared to the only direct numerical solution for the 3-D viscous fluid (22), in which computing times on 32 parallel processors for the linear solution of a single frequency are measured in hours. Without viscosity the computational problem is simplified. A number of laboratories now are computing passive cochlear waves in realistic cochlear models based on CT imaging, with the damping placed into the BM and without the organ of Corti.

RESULTS

BF-to-place Map

The passive model calculations of the best frequency (BF) versus place on the basilar membrane (*i.e.* the percentage of the total cochlea length, starting from the stapes) are shown in Figure S2 for four species (gerbil, chinchilla, cat, and human), along with corresponding measurements (23, 14, 16, 24). The computed and measured BF-to-place maps are in agreement to within 5% for each species except in the apical region of the cat cochlea, where the error is as large as 20% (Figure S2).

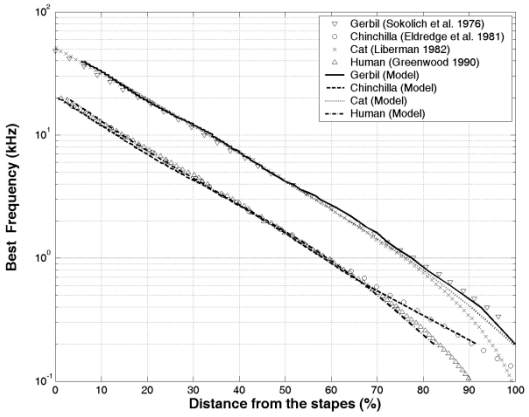

Figure S2: Best frequency (BF) versus percentage location along the cochlea for the interspecies 3-D cochlear model (lines) and corresponding measurements (symbols).

Pressure response near the BM

The calculated cochlear pressure P_C, near the basilar membrane on the scala tympani side, relative to the ear canal pressure P_{ec} is shown in Figure S3 for the passive (thin lines) and the active (thicker lines) cases. The simulated probe location is 10 μm, 15 μm, 21 μm and 35 μm from the basilar membrane for gerbil, chinchilla, cat and human, respectively. Only measurements for the gerbil cochlea by Olson (25), shown in first column, were available for comparison. The peak near the BF (20 kHz in gerbil) is due to the slow-wave pressure gain, while the flat portion above the BF is due to the fast-wave pressure. The oscillations are due to the interactions between the slow and fast waves.

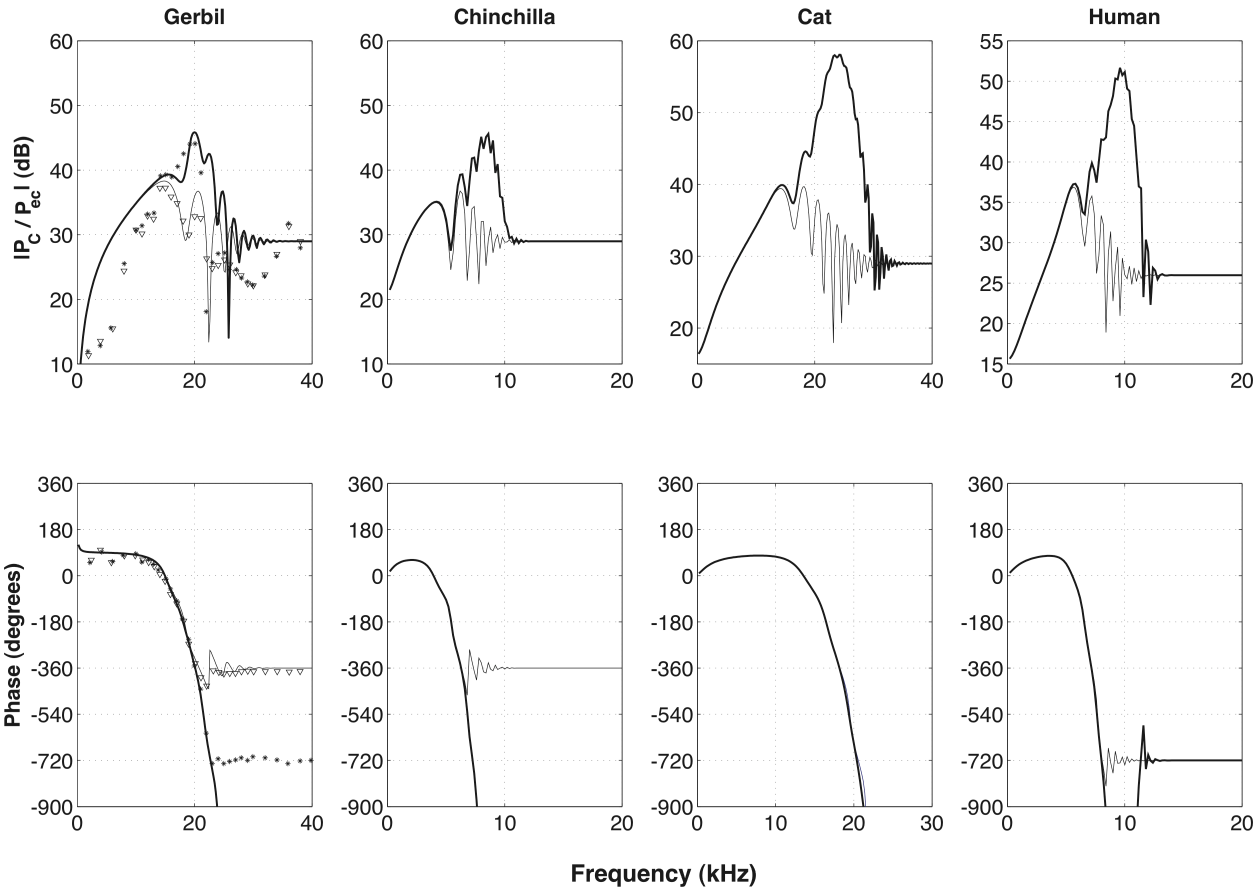

Figure S3: Cochlear pressure (P_C) near the basilar membrane on the scala tympani side, relative to ear-canal pressure (P_{ec}). The measurements for the gerbil cochlea are from Olson (25, Figure 7) with the probe 22 μm from the BM, and with input pressures of 50 dB SPL for the active case (*) and 80 dB SPL for the passive case (∇). The thin lines show the calculated P_C/P_{ec} transfer function for the passive case, while the thicker lines show the active case. The top row shows the magnitude of P_C/P_{ec} for gerbil (1st column), chinchilla (2nd column), cat (3rd column) and human (4th column) and the bottom row shows the corresponding phase.

SUPPORTING MATERIAL REFERENCES

1. Steele, C. R., and L. A. Taber. 1979. Comparison of WKB calculations and experimental results for three-dimensional cochlear models. *J. Acoust. Soc. Am.* 65:1007-1018.
2. Lim, K. M., and C. R. Steele. 2002. A three-dimensional nonlinear active cochlear model analyzed by the WKB-numeric method. *Hear. Res.* 170:190-205.

3. Yoon, Y., S. Puria, and C. R. Steele. 2007. Intracochlear pressure and derived quantities from a three-dimensional model. *J. Acoust. Soc. Am.* 122:952-966.
4. Yoon, Y., S. Puria, and C. R. Steele. 2009. A Cochlear model using the time-averaged Lagrangian and the push-pull mechanism in the organ of Corti. *J. Mech. Mat. Str.* 4: 977-986.
5. Wen, B. and K. Boahen. 2003. A linear cochlear model with active bi-directional coupling. The 25th Annual International Conference of the IEEE Engineering in Medicine and Biology Society (EMBC 2003). 2013-2016.
6. Iurato, S. 1962. Functional implications of the nature and submicroscopic structure of the tectorial and basilar membrane. *J. Acoust. Soc. Am.* 34:1386-1395.
7. Steele, C. R., G. Baker, J. Tolomeo, and D. Zetes. 1995. Cochlear Mechanics. The Biomedical Engineering Handbook Ed. Bronzino, ZD, CRC press. 505-516.
8. Dannhof, B. J., B. Roth, and V. Bruns. 1991. Length of hair cells as a measure of frequency representation in the mammalian inner ear. *Naturwiss.* 78: 570–573.54.
9. Edge, R. M., B. N. Evans, M. Pearce, C. P. Richter, X. Hu, and P. S. Dallos. 1998. Morphology of the unfixed cochlea. *Hear. Res.* 124:1-16.
10. Decraemer, W. F., S. M. Khanna, O. de La Rochefoucauld, W. Dong, J. J. J. Dirckx, and E. S. Olson. 2007. Scala vestibuli pressure and three-dimensional stapes velocity measured in direct succession in gerbil. *J. Acoust. Soc. Am.* 121: 2774-2791.
11. Naidu, R. C., and D. C. Mountain. 2007. Basilar membrane tension calculations for the gerbil cochlea. *J. Acoust. Soc. Am.* 121:994-1002.
12. Kim, N. K., Y. Yoon, S. Puria, and C. R. Steele. 2008. Cochlear scala areas and basilar membrane (BM) width with the straight and the bent modiolus using micro computed tomography (μCT) imaging. ARO MidWinter Meeting 144.
13. Dallos, P. 1970. Low-frequency auditory characteristics: Species dependence. *J. Acoust. Soc. Am.* 48:489-504.
14. Eldredge, D. H., J. D. Miller, and B. A. Bohne, 1981. A frequency-position map for the chinchilla cochlea. *J. Acoust. Soc. Am.* 69:1091-1095.
15. Cabezudo, L. M. 1978. The ultrastructure of the basilar membrane in the cat. *Acta Otolaryngol.* 86:160-175.
16. Liberman, M. C. 1982. The cochlear frequency map for the cat: Labeling auditory-nerve fibers of known characteristic frequency. *J. Acoust. Soc. Am.* 72:1441-1449.
17. Lynch, T. J., V. III Nedzelnitsky, and W. T. Peake. 1982. Input impedance of the cochlea in cat. *J. Acoust. Soc. Am.* 72:108-130.
18. Wever, E. G. 1949. Theory of hearing. John Wiley. New York.
19. von Békésy, G. 1960. Experiments in Hearing. McGraw-Hill. New York.
20. Thorne, M., A. N. Salt, J. E. DeMott, M. M. Henson, O. W. Jr. Henson, and S. L. Gewalt. 1999. Cochlear Fluid Space Dimensions for Six Species Derived From Reconstructions of Three-Dimensional Magnetic Resonance Images. *Laryngoscope*. 109:1661-1668.
21. Aibara, R., J. T. Welsh, S. Puria, and R. L. Goode. 2001. Human middle-ear sound transfer function and cochlear input impedance. *Hear. Res.* 152:100-109.
22. Givelberg, E. and J. Bunn. 2003. A comprehensive three-dimensional model of the cochlea. *J. Computational Physics* 191(2): 377-391.
23. Sokolich, W. G., R. P. Hamernik, J. J. Zwisiocki, and R. A. Schmiedt. 1976. lnferred response polarities of cochlear hair cells. *J. Acoust. Soc. Am.* 59:963-979.
24. Greenwood, D. D. 1990. A cochlear frequency-position function for several species-29 years later. *J. Acoust. Soc. Am.* 87:2592-2605.
25. Olson, E.S., *Intracochlear pressure measurements related to cochlear tuning.* J Acoust Soc Am, 2001. 110(1): p. 349-67.